Creating an Artificial Two-Dimensional Skyrmion Crystal by Nanopatterning

L. Sun, R. X. Cao, B. F. Miao, Z. Feng, B. You, D. Wu, W. Zhang, An Hu, and H. F. Ding*

National Laboratory of Solid State Microstructures and Department of Physics, Nanjing University, 22 Hankou Road, Nanjing 210093, People's Republic of China

(Received 31 December 2012; published 19 April 2013)

A Skyrmion crystal typically arises from helical spin structures induced by the Dzyaloshinskii-Moriya interaction. Experimentally its physical exploration has been impeded because it is a rarity and is found only within a narrow temperature and magnetic field range. We present a method for the assembly of a two-dimensional Skyrmion crystal based upon a combination of a perpendicularly magnetized film and nanopatterned arrays of magnetic vortices that are geometrically confined within nanodisks. The practical feasibility of the method is validated by micromagnetic simulations and computed Skyrmion number per unit cell. We also quantify a wide range in temperature and field strength over which the Skyrmion crystal can be stabilized without the need for any intrinsic Dzyaloshinskii-Moriya interactions, which otherwise is needed to underpin the arrangement as is the case in the very few known Skyrmion crystal cases. Thus, our suggested scheme involves a qualitative breakthrough that comes with a substantial quantitative advance.

DOI: 10.1103/PhysRevLett.110.167201 PACS numbers: 75.70.−i, 75.30.Kz, 75.60.Jk, 75.75.−c

The Skyrmion spin structure is a topologically stable state in which the spins point in all directions wrapping a sphere [1,2]. The Skyrmion configuration in a magnetic solid carries a topological charge and a Berry phase in real space. It is anticipated to produce unconventional spin-electronic phenomena, such as the topological Hall effect [3–6] and to exhibit spectacular dynamic properties [7–9]. Technologically, the Skyrmion crystal may be exploited as a new class of spintronic materials due to its unusual response to the electric charge current and spin current [10,11]. The Skyrmion crystal also attracts interdisciplinary interest as an analog of similar lattice structures in nuclear physics [2,12], quantum Hall systems [13,14], and liquid crystals [15]. Experimentally, neutron scattering studies confirmed the existence of the Skyrmion crystal within a narrow temperature or field region on the three-dimensional (3D) helical magnets MnSi [16] and $Fe_{1-x}Co_xSi$ [17]. The real-space spin configuration of the 2D Skyrmion lattice was recently revealed by Lorentz transmission electron microscopy in thin films of $Fe_{0.5}Co_{0.5}Si$, MnSi, and FeGe [10,18,19]. It shows ordered hexagonal arrays of vortices that bear the same polarity and chirality, and that are surrounded by perpendicular domains with the magnetization aligned oppositely to that of the vortex cores. It was found that the 2D Skyrmion crystal can exist in a wider temperature or field range in comparison with 3D lattices [6,18]. The rarity and the narrow temperature-field region of the existence of the Skyrmion crystal impede exploration of its physical properties. Particularly, to date, no Skyrmion crystal has been found at room temperature. In addition, a Skyrmion crystal typically arises from helical spin structures induced by the Dzyaloshinskii-Moriya (DM) interaction [20,21]. The DM interaction, however, is commonly weak, limiting the material selection of Skyrmion crystals.

In this Letter we present a novel approach for creating a 2D Skyrmion crystal. It is alternative to the heretofore explored path of, essentially, synthesizing a material with as high an intrinsic DM interaction as possible. In contrast to the bottom-up approach of looking to have a grip on a truly microscopic mechanism (DM), our proposal is top-down in that a combination of established thin-film growth techniques, nanopatterning, and knowledge of macroscopic ferromagnetic characteristics of thin layers is implemented, resulting in the blueprint for the practical assembly of an artificial structure with the desired properties. The artificial Skyrmion crystal thus assembled does not depend on the presence of DM interactions in the assembly components. Geometrically, the magnetic configuration of a 2D Skyrmion crystal can be considered as hexagonal arrays of vortices surrounded by perpendicular domains, where the vortex state typically can be stabilized within micron- or nanosized disks [22]. We therefore combine patterned arrays of magnetic nanodisks with a magnetic film that has perpendicular anisotropy. The approach is demonstrated with micromagnetic simulations utilizing the OOMMF code [23] and computed Skyrmion number per unit cell. Our Skyrmion crystal can be stabilized in a wide temperature and field range, even at room temperature and zero magnetic field, and in the absence of the DM interaction, which significantly widens the scope of potential material systems and practical applications.

Figure 1 presents the proposed pathway for creating the 2D Skyrmion crystal. First, a film with perpendicular anisotropy is prepared. The second step is to fabricate ordered arrays of nanosized magnetic disks on top of the film. This can be achieved utilizing advanced patterning techniques, such as *e*-beam lithography and focused ion beam approaches. With proper selection of the aspect ratio between the diameter and thickness, the disks can be

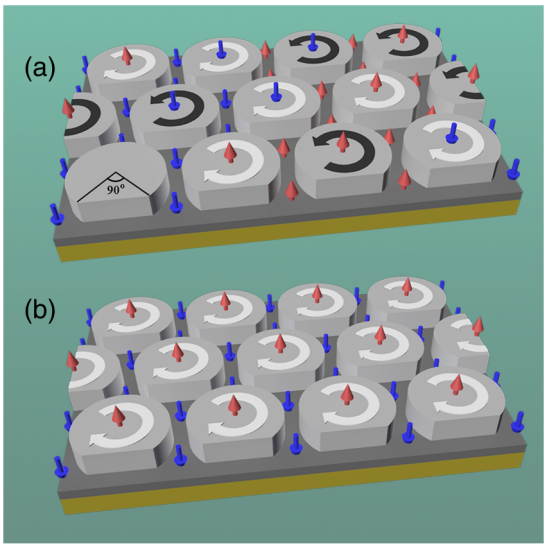

FIG. 1 (color online). Proposed pathway for creating the 2D Skyrmion crystal. (a) Ordered arrays of magnetic submicron disks are prepared on top of a film with perpendicular anisotropy. The arrows represent the magnetization orientation of the local moments. (b) Skyrmion lattice creation with the field treatment mentioned in the text.

magnetically configured into vortex states according to the known magnetic phase diagram [24,25]. Because of the random distribution, the vortices would naturally have different chirality and polarity as shown in Fig. 1(a). The Skyrmion lattice requires all the vortices to bear the same chirality and polarity [18]. Therefore, the third step is to format all the vortices into the same configuration with the magnetization of the vortex cores oppositely aligned with the disk surrounding are as shown in Fig. 1(b). In such a case, a Skyrmion crystal can be created. As will be demonstrated below, this can be achieved by the combination of slight disk shape modification and specific magnetic field treatments. In this study, we use edge-cut circular disks with the cutting angle of 90° [see the left disk of the front row shown in Fig. 1(a)], similar to that in Ref. [26]. All disks are cut along the same direction.

In the following, we will discuss the feasibility of the proposal utilizing micromagnetic simulations. Co is chosen as the disk material as it has a vortex state under similar geometrical confinement conditions [25]. For the perpendicular film, CoPt film is used because it has a high perpendicular anisotropy and is conductive starting from a thickness of a few nm [27]. The material parameters used in calculations are exchange constant: $A^{\mathrm{Co}} = 2.5 \times 10^{-11}$ J/m; saturation magnetization: $M_S^{\mathrm{Co}} = 1.4 \times 10^6$ A/m for Co [17]; and $A^{\mathrm{CoPt}} = 1.5 \times 10^{-11}$ J/m, $M_S^{\mathrm{CoPt}} = 5.0 \times 10^5$ A/m for CoPt [28,29]. A uniaxial anisotropy perpendicular to the film with constant $K_1^{\mathrm{CoPt}} = 4.0 \times 10^5$ J/m^3 is included for CoPt [29]. Because sputtered Co films are typically polycrystalline, we performed the calculations assuming zero anisotropy. The calculations also assumed the single crystalline magnetic anisotropy value for bulk Co. This only slightly changes the size of the vortex cores. An interlayer exchange constant between Co and CoPt of 1.9×10^{-11} J/m is also used [23]. The disks with diameter D and thickness t_d are aligned into hexagonal arrays. In addition, the separation between centers of disks is S. In the calculations, we used 2D periodical boundary conditions within the plane and a grid size of $2 \times 2 \times 1$ nm^3, which is smaller in length scale than the exchange length of Co (≈ 11 nm) and CoPt (≈ 5 nm). As a starting point, we chose disks with $D = 120$ nm and $t_d = 18$ nm, the CoPt film with thickness $t_f = 8$ nm, and the separation $S = 150$ nm, which is close in size to the Skyrmion crystal geometry reported in Ref. [18]. With the initial random spin configuration, the results show the disks are partially in vortex states and partially in C states. This is due to the dimensions of the disks being within the bistable region even though the vortex state has lower energy [25]. The polarity and chirality of the vortices are randomly distributed, similar to that shown in Fig. 1(a). To format all the disks into uniform vortices, we proceed with a magnetic field treatment similar to that reported in Ref. [30]. We first apply a field of 800 mT perpendicular to the disks to bring them into the vortex state with the same polarity. Then we add an in-plane field pulse of 400 mT along the cutting edge to configure them into the same chirality. After releasing the perpendicular field, we find that all the disks are indeed formatted into uniform vortices of the same polarity and chirality.

During the formatting of the vortex, we find that the disk surrounding areas are also magnetized in the same direction of the vortex core due to the applied strong field. A Skyrmion crystal, however, requires the magnetization orientation of the vortex core and the vortex surrounding area aligned oppositely. Therefore, we further apply a magnetic field with the opposite direction. Remarkably, we find that the vortex core and the disk surrounding area can have different switching fields. Figure 2 presents the calculated zero-field configuration after applying a field of 400 mT. We find that indeed the CoPt film surrounding the disk can be uniformly magnetized oppositely with the vortex core and without significantly influencing the vortex configuration. Thus, a Skyrmion crystal is created. With the exchange constant and the disk size, one could also estimate an effective DM interaction constant [18]. We find it is in the order of 10^{-3} J/m^2 for the sample discussed above.

To explore topological properties of this artificial Skyrmion crystal, we computed its local Skyrmion density ϕ following the description given in Ref. [16]. If ϕ integrates to 1 or -1 in a unit cell, a topologically stable knot exists in the magnetization. As shown in Fig. 3(a), the Skyrmion density is finite and oscillates as a function of the position, similar to that shown in Ref. [16]. Moreover,

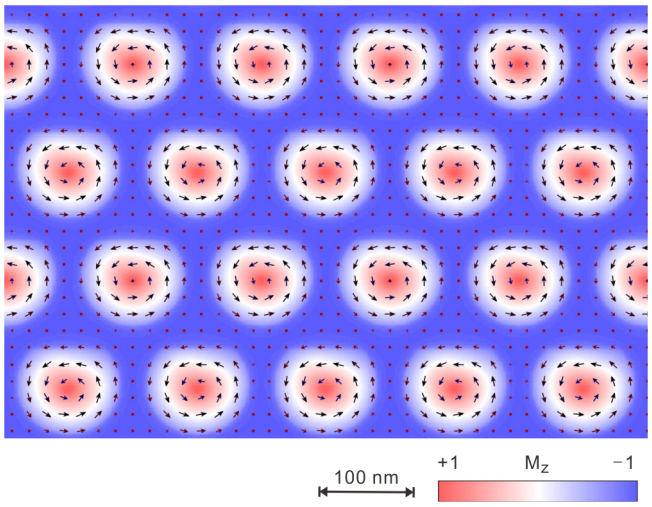

FIG. 2 (color online). Top view of magnetic configuration of the CoPt layer in a calculated artificial Skyrmion crystal at zero field. (Co disk size: $D = 120$ nm and $t_d = 18$ nm; CoPt film thickness $t_f = 8$ nm.) The arrows represent the magnetization orientation of the local moments.

the Skyrmion number per 2D unit cell is quantized and adds up to $+1$, proving the topological nature of the created artificial Skyrmion crystal. This can also be understood within a qualitative picture. When a unit cell is split by a boundary where the magnetization is fully in plane [the black circle in Fig. 3(b)], it can be considered as a combination of a vortex with the core pointing up [the green area in Fig. 3(b)] and a distorted antivortex whose core magnetization points down [outside the green area in Fig. 3(c)]. We note the distorted antivortex is not a typical antivortex that has a cross configuration [31]. But one can readily derive that it has a winding number of -1 and the polarity of -1, yielding a Skyrmion number (defined as half of the product of the winding number and the polarity) of $1/2$. Together with the contribution of the vortex with opposite polarity, a unit cell has a Skyrmion number of $+1$. The fact that a vortex and an antivortex with *antiparallel* core polarizations have equal Skyrmion numbers adding to a total of $+1$ or -1 was previously pointed out by Tretiakov and Tchernyshyov [32].

We continue to discuss the stability of the artificial Skyrmion crystal. In the calculations, the material parameters of Co and CoPt at room temperature are used. Given the strong magnetic anisotropy of CoPt and the film thickness, it would be expected that the system has a Curie temperature T_C close to its bulk value. Therefore, the magnetic configuration could survive from low temperature to close to T_C, which is well above room temperature. To explore its stability in field, we also performed calculations in various strength magnetic fields. Figure 4 presents the calculated phase diagram and the field-dependent vortex core diameter, d, which is defined as the full width of the half value of the magnetization in

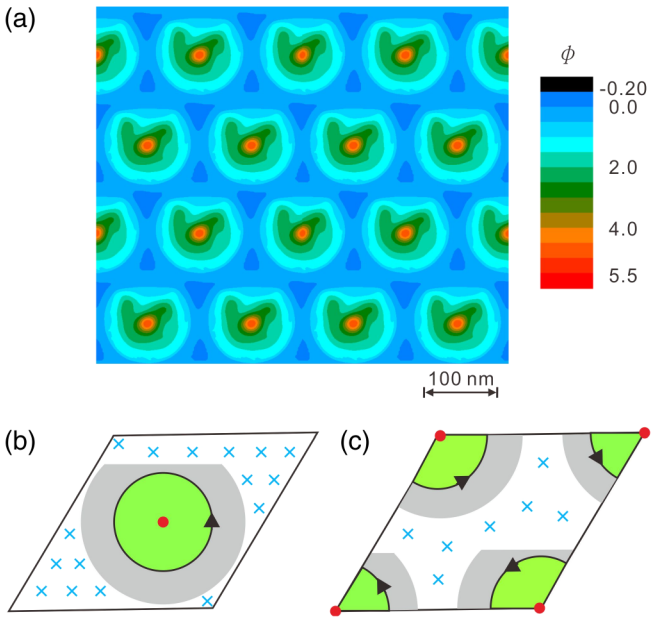

FIG. 3 (color online). (a) Calculated local Skyrmion density per unit cell for the artificial Skyrmion crystal shown in Fig. 2. (b) Schematic picture of a vortex with core magnetization pointing up (the green area). (c) Schematic picture of a distorted antivortex with core magnetization pointing down (outside the green area). The black arrows represent the in-plane magnetization orientation. The red dots and blue crosses indicate that magnetization pointing up and down, respectively.

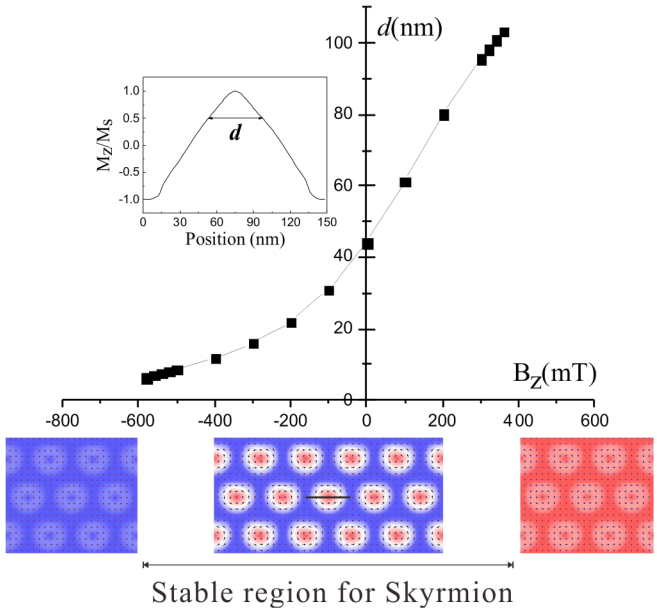

FIG. 4 (color online). Calculated phase diagram and the core diameter of vortex in Skyrmion configuration as a function of perpendicular field. The detailed dimension is the same as in Fig. 2. Inset shows the typical magnetization line profile across a vortex center as marked at the bottom.

the perpendicular direction (see the inserted line profile in Fig. 4). We find that the stability of the Skyrmion crystal depends on the direction of the applied field. When the field is applied along the vortex core direction, the crystal can be stabilized until the film magnetization is switched. When the field is applied oppositely, the Skyrmion crystal is stable until the flipping of the vortex polarity. In between, the system remains in a Skyrmion state. In this particular geometry, we find that the Skyrmion crystal can be stable in a wide field range, from about -580 to $+360$ mT. We note that the stability also depends on the sizes of the disks and their separation, as well as the film thickness. Interestingly, we find that the vortex core size also depends on the external field. Figure 4 presents the field dependence of the vortex core diameter. We find that the vortex core expands when the field is parallel to the magnetization of the vortex core and shrinks when the field is applied oppositely. This can be understood as follows. The vortex core size is determined by the competition among the exchange energy, the dipolar energy, and the perpendicular anisotropy energy. The perpendicular external field can be considered as a unidirectional anisotropy. Depending on its orientation, the field can enhance or decrease the effective anisotropy and result in a change of the vortex core size accordingly. We note that we did not observe the dip zone that is commonly found surrounding a usual vortex core in a soft disk [33]. It could be related to the fact that the disks are surrounded by the area with the magnetization aligned oppositely with the vortex core in our case.

The stability of the Skyrmion is also explored as the function of both the film and disk thickness, and it is found that it can be stabilized in a broad region as shown in Fig. 5. For $D = 120$ nm and $S = 150$ nm, Fig. 5(a), it exists in most of the combination of the film and disk thickness when $t_d > 20$ nm. Below that, the disks and the area under them are in C states. Interestingly, we find that the switching of vortex cores and the disk surrounding area are thickness dependent. When $t_f > 10$ nm, the polarities of the vortices are switched before the disk surrounding area, resulting in a Skyrmion lattice with opposite Skyrmion density per unit cell. Figure 5(b) presents the phase diagram for $D = 90$ nm and $S = 100$ nm. The stable region is slightly smaller. This can be understood that the disks have the tendency to form a C state with decreasing size. The stability is also examined for larger dimensions, e.g., $D = 800$ nm and $S = 900$ nm and the Skyrmion crystal was also obtained. Additional calculations are made for the combination of Co disks and FePt film; the Skyrmion state can also be found with proper geometrical configuration.

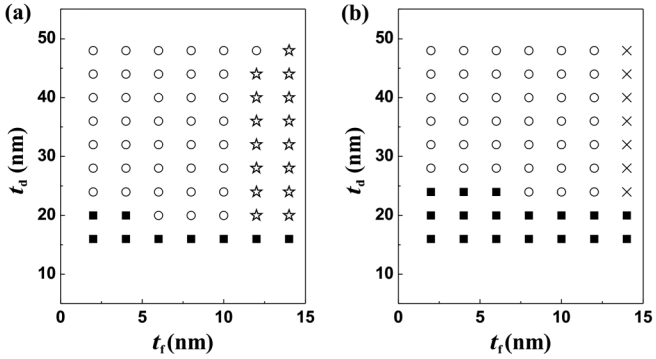

FIG. 5. Calculated phase diagram of the Skyrmion stability for systems with (a) $D = 120$ nm and $S = 150$ nm, (b) $D = 90$ nm and $S = 100$ nm. Black squares represent disks in C states. The open circles and stars show the systems in Skyrmion states with $+1/-1$ Skyrmion density per unit cell, respectively. The cross represents the systems in states with partially Skyrmion and partially topologically normal state (the vortex core and the magnetization of the disk surrounding area are pointing to the same direction).

In the few experimental cases of Skyrmion crystals known at this time [10,16–19], only the densely packed hexagonal Skyrmion pattern with a fixed (naturally emerging) period is found. In contrast, the artificial Skyrmion crystal created by the geometric confinement may offer additional advantages besides the stability discussed above. For instance, the lattice constant can be controllably varied and even different patterns may be artificially designed and realized by means of advanced lithography techniques. Electrically, the topological Hall effect was observed in the DM-driven Skyrmion crystals [3–6]. In the artificial Skyrmion crystal discussed in this Letter, the nanodisks are only electrically connected by the CoPt film. They should have no significant influence on the electrical properties of the Skyrmion crystal. Thus, the topological Hall effect should be expected. Moreover, we find that the artificial Skyrmion crystals, upon field excitation, have similar dynamic modes as the naturally formed Skyrmion crystals, such as rotational and breathing modes [8,9].

In summary, we present a method for creating 2D artificial Skyrmion crystals with a combination of perpendicularly magnetized film and nanopatterned arrays of uniform magnetic vortices. The idea is similar to a simulation of spin ice systems with artificially frustrated magnets [34,35]. The method is demonstrated with micromagnetic simulations and the computed Skyrmion number per unit cell. The created Skyrmion crystal can be stabilized in a wide temperature and field range, even at room temperature, zero magnetic field, and in the absence of the DM interaction. It can significantly widen the scope of properties exploration and practical applications of Skyrmion crystals. For instance, the topological nature of the created Skyrmion crystal may protect itself against the thermal fluctuation better than the usual nanomagnets, casting its potential application in future data storage [36]. We note that, from a more general point of view, previous experimental and theoretical studies of systems with DM interactions have already shown amply that the DM interaction is not sufficient for the spontaneous formation of a

Skyrmion crystal all by itself, since many systems with DM interaction do not display Skyrmion crystal self-assembly. Our method demonstrates that the DM interaction is not necessary either.

This work is supported by the State Key Programme for Basic Research of China (Grants No. 2010CB923401 and No. 2011CB922103), NSFC (Grants No. 10834001, No. 10974087, and No. 11023002), Natural Science Foundation of Jiangsu (Grant No. BK2012300), and PAPD.

*Corresponding author.
hfding@nju.edu.cn

[1] T. H. R. Skyrme, Proc. R. Soc. A **262**, 237 (1961).
[2] T. H. R. Skyrme, Nucl. Phys. **31**, 556 (1962).
[3] Y. Onose, N. Takeshita, C. Terakura, H. Takagi, and Y. Tokura, Phys. Rev. B **72**, 224431 (2005).
[4] A. Neubauer, C. Pfleiderer, B. Binz, A. Rosch, R. Ritz, P. G. Niklowitz, and P. Böni, Phys. Rev. Lett. **102**, 186602 (2009).
[5] M. Lee, W. Kang, Y. Onose, Y. Tokura, and N. P. Ong, Phys. Rev. Lett. **102**, 186601 (2009).
[6] S. X. Huang and C. L. Chien, Phys. Rev. Lett. **108**, 267201 (2012).
[7] O. Petrova and O. Tchernyshyov, Phys. Rev. B **84**, 214433 (2011).
[8] M. Mochizuki, Phys. Rev. Lett. **108**, 017601 (2012).
[9] Y. Onose, Y. Okamura, S. Seki, S. Ishiwata, and Y. Tokura, Phys. Rev. Lett. **109**, 037603 (2012).
[10] X. Z. Yu, N. Kanazawa, W. Z. Zhang, T. Nagai, T. Hara, K. Kimoto, Y. Matsui, Y. Onose, and Y. Tokura, Nat. Commun. **3**, 988 (2012).
[11] F. Jonietz, S. Mühlbauer, C. Pfleiderer, A. Neubauer, W. Münzer, A. Bauer, T. Adams, R. Georgii, P. Böni, R. A. Duine, K. Everschor, M. Garst, and A. Rosch, Science **330**, 1648 (2010).
[12] I. Klebanov, Nucl. Phys. **B262**, 133 (1985).
[13] S. L. Sondhi, A. Karlhede, S. A. Kivelson, and E. H. Rezayi, Phys. Rev. B **47**, 16 419 (1993).
[14] L. Brey, H. A. Fertig, R. Côté, and A. H. MacDonald, Phys. Rev. Lett. **75**, 2562 (1995).
[15] A. N. Bogdanov, U. K. Rößler, and A. A. Shestakov, Phys. Rev. E **67**, 016602 (2003).
[16] S. Mühlbauer, B. Binz, F. Jonietz, C. Pfleiderer, A. Rosch, A. Neubauer, R. Georgii, and P. Böni, Science **323**, 915 (2009).
[17] W. Münzer, A. Neubauer, T. Adams, S. Mühlbauer, C. Franz, F. Jonietz, R. Georgii, P. Böni, B. Pedersen, M. Schmidt, A. Rosch, and C. Pfleiderer, Phys. Rev. B **81**, 041203(R) (2010).
[18] X. Z. Yu, Y. Onose, N. Kanazawa, J. H. Park, J. H. Han, Y. Matsui, N. Nagaosa, and Y. Tokura, Nature (London) **465**, 901 (2010).
[19] X. Z. Yu, N. Kanazawa, Y. Onose, K. Kimoto, W. Z. Zhang, S. Ishiwata, Y. Matsui, and Y. Tokura, Nat. Mater. **10**, 106 (2011).
[20] I. Dzyaloshinsky, J. Phys. Chem. Solids **4**, 241 (1958).
[21] T. Moriya, Phys. Rev. **120**, 91 (1960).
[22] A. Hubert and R. Schäfer, *Magnetic Domains: The Analysis of Magnetic Microstructures* (Springer, New York, 2000).
[23] M. J. Donahue and D. G. Porter, *OOMMF User's Guide Version 1.0* (National Institute of Standards and Technology, Gaithersburg, MD, 1999).
[24] R. P. Cowburn, D. K. Koltsov, A. O. Adeyeye, M. E. Welland, and D. M. Tricker, Phys. Rev. Lett. **83**, 1042 (1999).
[25] H. F. Ding, A. K. Schmid, D. Li, K. Y. Guslienko, and S. D. Bader, Phys. Rev. Lett. **94**, 157202 (2005).
[26] R. K. Dumas, T. Gredig, C.-P. Li, I. K. Schuller, and K. Liu, Phys. Rev. B **80**, 014416 (2009).
[27] J. Moritz, B. Rodmacq, S. Auffret, and B. Dieny, J. Phys. D **41**, 135001 (2008).
[28] C. Eyrich, W. Huttema, M. Arora, E. Montoya, F. Rashidi, C. Burrowes, B. Kardasz, E. Girt, B. Heinrich, O. N. Mryasov, M. From, and O. Karis, J. Appl. Phys. **111**, 07C919 (2012).
[29] M. Maret, M. C. Cadeville, R. Poinsot, A. Herr, E. Beaurepaire, and C. Monier, J. Magn. Magn. Mater. **166**, 45 (1997).
[30] Z. Pang, F. Yin, S. Fang, W. Zheng, and S. Han, J. Magn. Magn. Mater. **324**, 884 (2012).
[31] R. Hertel and C. M. Schneider, Phys. Rev. Lett. **97**, 177202 (2006).
[32] O. A. Tretiakov and O. Tchernyshyov, Phys. Rev. B **75**, 012408 (2007).
[33] J. K. Ha, R. Hertel, and J. Kirschner, Phys. Rev. B **67**, 224432 (2003).
[34] R. F. Wang, C. Nisoli, R. S. Freitas, J. Li, W. McConville, B. J. Cooley, M. S. Lund, N. Samarth, C. Leighton, V. H. Crespi, and P. Schiffer, Nature (London) **439**, 303 (2006).
[35] Y. Qi, T. Brintlinger, and J. Cumings, Phys. Rev. B **77**, 094418 (2008).
[36] N. S. Kiselev, A. N. Bogdanov, R. Schäfer, and U. K. Rößler, J. Phys. D **44**, 392001 (2011).